Dalton Transactions

Accepted Manuscript

ROYAL SOCIETY OF CHEMISTRY

rsc.li/dalton

View Article Online
DOI: 10.1039/C8DT00500A

Dalton Transactions

ARTICLE

Silver Metal Complex as a Luminescent Probe for Enzymatic Sensing of Blood Plasma Glucose and Urine

Received 00th January 20xx,
Accepted 00th January 20xx

DOI: 10.1039/x0xx00000x

www.rsc.org/

Zheng-Bang Pan,[a] Ying-Chu Wang,[a] Gomathy Chakkaradhari,[b] Jian Fan Zhu,[a] Rong-Yu He,[a] Yu-Ci Liu,[a] Chia-Hui Hsu,[a] Igor O. Koshevoy,*[b] Pi-Tai Chou,*[c] Sheng-Wei Pan[d,e,f] and Mei-Lin Ho*[a]

In this work, we present a facile preparation of a paper-based glucose assay for rapid, sensitive, and quantitative measurement in blood plasma and urine. Two copper phosphorescent complexes [Cu(2,9-dimethyl-4,7-diphenyl-1,10-phenanthroline)(2,6-dimethylphenylisocyanide)$_2$][B(C$_6$H$_3$(CF$_3$)$_2$)$_4$] (**Cu1**), [Cu(2,9-dimethyl-1,10-phenanthroline)(2,6-dimethylphenylisocyanide)$_2$][B(C$_6$H$_3$(CF$_3$)$_2$)$_4$] (**Cu2**) and a new silver congener [Ag(P^3)CNAg(P^3)][B(C$_6$H$_3$(CF$_3$)$_2$)$_4$] (**Ag3**) (P^3 = PPh$_2$C$_6$H$_4$–PPh–C$_6$H$_4$PPh$_2$ [bis(*o*-diphenylphosphinophenyl)phenylphosphine]) have been synthesized and their oxygen sensing abilities were investigated. The dimetallic phosphine-based **Ag3** complex, having high oxygen sensing ability, was employed as an efficient signal transducer in enzymatic reactions to recognize blood plasma glucose and urine glucose, which provided a wide linear response for a concentration range between 1.0 and 35 mM and a rapid response, with a limit of detection (LOD) for glucose of 0.09 mM. In practical application, this **Ag3** paper-based device offers great analytical reliability and accuracy upon monitoring glucose concentrations in blood plasma.

Introduction

Optical oxygen and glucose probes are appealing in food, industrial safety and health control.[1,2] Optical sensors provide several promising features over electrochemical-based meters. They can detect analytes in matrices with minimal sample pre-treatment, allow real-time continuous monitoring and provide important information about the biomolecular structures and environments associated with healthy and diseased states. Also they are free of electromagnetic disturbances.[3] Combining the optical probe with modern microelectronics and optoelectronics, such as mobile phones and fiber optics, offers powerful devices for sensing in several fields.[1,4] Moreover, optical probes loaded on the cellulose paper to construct paper-based analytical tools have shown great potential in the development of point-of-care tests.[5]

Glucose is one of the most popular analytes in the research field because abnormal levels of glucose are related to diabetes, a chronic metabolic disease influencing a great population of people worldwide.[6] Numerous luminescence materials have been used for glucose detection, including Au nanodots,[7] Eu^{3+}-doped $GdVO_4$,[8] fluorescein isothiocyanate,[9] $NaYF_4$:Yb^{3+}/Er^{3+},[10] GQDs,[11,12] Ir-Zn_e,[13] CdSe/ZnS,[14] and rhodamine derivatives.[15] For healthy humans, concentrations of glucose in the blood and urine of *ca.* 4.4–6.6 mM and 0.1–0.8 mM, respectively, are normally detected.[16] According to the American Diabetes Association, for diabetics, the blood glucose concentration should be maintained below 10 mM (180 mg/dl).[5]

An optical glucose sensing system contains three main parts: (i) a recognition part: an element to selectively recognize an analyte in the matrix, (ii) a transducer part: an element that can convert the recognition signal from the probe into a measurable signal, and (iii) a signal processing part: a system that converts the signal into a readable format.[17] A number of aspects concerning these three parts need to be considered in order to optimize the development of biosensors, including easy for preparation and use, provision of fast response, accuracy, sensitivity and selectivity and simultaneously the miniaturization of the instruments.[1]

Transition-metal complexes with the d^{10} electron configuration are known to demonstrate tunable optical properties. Among these, M^I (M = Cu, Ag, Au) compounds show diverse coordination behavior with respect to a wide range of ionic and neutral ligands to give numerous materials, which exhibit intriguing thermo-, vapo-, and mechanochromic luminescence.[18-25] Recently, the utilization of a chelating triphosphine ligand, PPh$_2$C$_6$H$_4$–PPh–C$_6$H$_4$PPh$_2$ [bis(*o*-diphenylphosphinophenyl)phenylphosphine, P^3], to prepare a series of metalloligand complexes M(P^3)CN and their di- and

[a] Department of Chemistry, Soochow University, No 70, LinShih Rd., Shih-Lin, Taipei 11102, Taiwan. Fax: +886-2-28811053; Tel: +886-2-28819471 ext. 6827; E-mail: meilin_ho@scu.edu.tw.
[b] University of Eastern Finland, Department of Chemistry, 80101, Joensuu, Finland. E-mail: igor.koshevoy@uef.fi
[c] National Taiwan University, Department of Chemistry, Taipei 106, Taiwan. E-mail: chop@ntu.edu.tw
[d] Department of Chest Medicine, Taipei Veterans General Hospital, Taipei, Taiwan.
[e] School of Medicine, National Yang-Ming University, Taipei, Taiwan.
[f] Institute of Public Health, National Yang-Ming University, Taipei, Taiwan.
Electronic Supplementary Information (ESI) available: The photoresponse of complex **Ag3** for detection glucose in air and in solution. The Lineweaver–Burk plot of the reciprocal of the Michaelis–Menten equation and storage stability of the biosensor. See DOI: 10.1039/x0xx00000x

View Article Online
DOI: 10.1039/C8DT00500A

trimetallic derivatives has been reported.[21] The resulting compounds exhibit moderate-to-intense room temperature solid state photoluminescence. Their emission is mainly governed by metal-to-ligand charge transfer transition mixed with some ligand-to-ligand charge transfer. More importantly, the crystalline bimetallic species have been shown to demonstrate very high sensitivity of luminescence characteristics to molecular oxygen.

In this contribution, we present the comparative analysis of two copper phosphorescent complexes **Cu1**, **Cu2** and a novel silver congener **Ag3** (Chart 1) for the purpose of sensing molecular oxygen, blood plasma glucose and urine. From the viewpoint of sensitivity and stability, the dimetallic phosphine-based **Ag3** complex is successfully employed as an efficient transducer in enzymatic reactions to recognize glucose in blood plasma and urine. The success of this proof-of-concept relies on the high oxygen sensing ability of **Ag3**, even in the form of an amorphous phase, which offers the advantages of simplifying the overall preparation of a glucose assay, and a wide range of glucose concentrations to be monitored (1.0-35 mM). This system has proven to possess higher sensitivity and better selectivity than previously reported works. Detail of results and discussion is elaborated as follows.

Experimental

2.1.[Cu(2,9-dimethyl-4,7-diphenyl-1,10-phenanthroline)(2,6-dimethylphenylisocyanide)$_2$] [B($C_6H_3(CF_3)_2)_4$] (Cu1).

$[Cu(NCMe)_4]PF_6$ (150 mg, 0.402 mmol) was dissolved in dichloromethane (20 cm^3), and 2,9-dimethyl-4,7-diphenyl-1,10-phenanthroline (144 mg, 0.400 mmol) was added, followed by 2,6-dimethylphenylisocyanide (105 mg, 0.802 mmol). The pale yellow solution was stirred for 1 h. Then an excess of diethyl ether was added, causing precipitation of a nearly colourless solid of [Cu(2,9-dimethyl-4,7-diphenyl-1,10-phenanthroline)(2,6-dimethylphenylisocyanide)$_2$]PF_6, which was collected, washed with diethyl ether and dried (310 mg, 93%). This intermediate product was dissolved in dichloromethane (10 cm^3), and a solution of $Na[B(C_6H_3(CF_3)_2)_4]$ (350 mg, 0.395 mmol) in diethyl ether (10 cm^3) was added, causing the formation of a pale solid. The opaque mixture was stirred for 2 h and evaporated to dryness, after which the product was extracted with diethyl ether (3×10 cm^3). The extracts were filtered and concentrated to ca. 10 cm^3. An excess of methanol was added, resulting in pale yellow precipitate of **Cu1**, which was collected, washed with methanol and vacuum dried (450 mg, 90%). ^{1}H NMR (CD_2Cl_2; 298 K; δ): 8.01 (s, 2H), 7.82 (s, 2H), 7.75 (m, 8H, $B(C_6H_3(CF_3)_2)_4$), 7.65–7.60 (m, 5H, Ph), 7.57 (m, 4H, $B(C_6H_3(CF_3)_2)_4$), 7.30 (t, J_{HH} 7.6 Hz, 2H, isocyanide), 7.17 (d, J_{HH} 7.6 Hz, 2H, isocyanide), 3.25 (s, 6H), 2.41 (s, 12H). Anal. Calcd for $C_{76}H_{50}BCuF_{24}N_4$: C, 58.91; H, 3.25; N, 3.62. Found: C, 59.20; H, 3.31; N, 3.39. Complex [Cu(2,9-dimethyl-1,10-phenanthroline)(2,6-dimethylphenylisocyanide)$_2$][$B(C_6H_3(CF_3)_2)_4$] (**Cu2**) was synthesized according to the published procedure.[26]

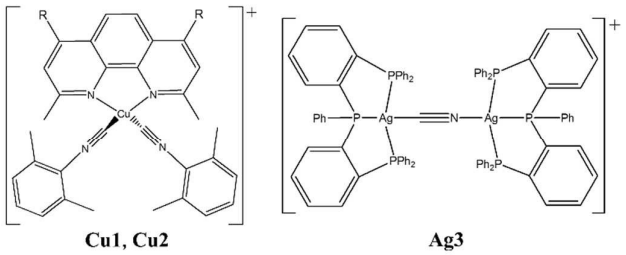

Cu1, Cu2 **Ag3**

Cu1: R = Ph; Cu2: R = H; Anions:$(B(C_6H_3(CF_3)_2)_4)^-$

Chart 1. Structures and abbreviations for Complexes.

2.2. [Ag(P^3)CNAg(P^3)][B($C_6H_3(CF_3)_2)_4$] (Ag3)

Ag3 was prepared by counterion metathesis from the [Ag(P^3)CNAg(P^3)]BF_4 complex.[21] [Ag(P^3)CNAg(P^3)]BF_4 (200 mg, 0.126 mmol) was dissolved in dichloromethane (10 cm^3) and treated with a solution of $Na[B(C_6H_3(CF_3)_2)_4]$ (123 mg, 139 mmol) in diethyl ether (10 cm^3). The opaque mixture was stirred for 2 h and evaporated to dryness, after which the product was extracted with diethyl ether (3×8 cm^3). The extracts were filtered and concentrated to ca. 5 cm^3, and an excess of hexanes was added slowly to produce pale flaky precipitate, which was collected, washed with pentane and vacuum dried (217 mg, 73%). The signals of the P^3 ligands in the ^{1}H and ^{31}P NMR spectra of **Ag3** are completely identical to those of [Ag(P^3)CNAg(P^3)]BF_4.[21] In addition, the compound demonstrates broadened ^{1}H resonances at 7.75 (m, 8H) and 7.58 (m, 4H) ppm (CD_2Cl_2), which correspond to $[B(C_6H_3(CF_3)_2)_4]^-$ counterion. Calcd for $C_{117}H_{78}Ag_2BF_{24}NP_6$: C, 59.39; H, 3.32; N, 0.59. Found: C, 59.67; H, 3.55; N, 0.49.

2.3. Chemical and reagents

Glucose oxidase (GOx, EC 1.1.3.4 from Aspergillus Niger) with a specific activity of 1 529 80 U g^{-1} of lyophilized solid, D-(+)-glucose (99%), D-fructose (99%), maltose monohydrate (99%), L-lysine (≧99.8), L-cysteine (≧99.8%), glutathione (≧98%), L-phenylalanine (≧98.5%), galactose (99%), lactose (99%), ascorbic acid (99%), citric acid (99%), uric acid (99%), albumin from human serum (HSA, ≧96%), glycine (≧99.7%) IgG (from human serum, ≧95%), potassium chloride (≧99.5%), magnesium dichloride (≧99.8%), L-tryptophan (≧98%), L-methionine (≧98%), L-aspartic acid (≧98%), L-valine (≧99%), and lauric acid (≧99%) were purchased from Sigma-Aldrich. Sodium chloride (99.8%) and calcium chloride dehydrate (≧99%) were obtained from J.T. Baker. Sodium fluoride (NaF, 99%) and ethylenediaminetetraacetic acid (EDTA, 98% ~ 110%) were purchased from Alfa aesar and Riedel-deHaën, respectively. All of the chemicals were used without further purification.

2.4. The measurement of oxygen collision efficiency

The oxygen collision efficiencies of **Cu1**, **Cu2** and **Ag3** on paper were evaluated based on the principle of luminescence intensity quenching. The **Cu1**, **Cu2** and **Ag3** in methanol solution (10^{-3} M) were dropped on the filter papers, which

View Article Online
DOI: 10.1039/C8DT00500A

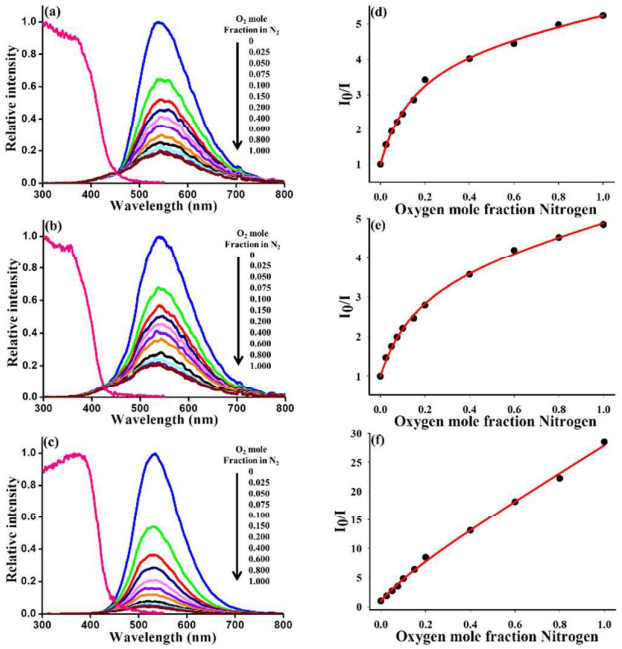

Figure 1. The responses of **Cu1** (a), **Cu2** (b) and **Ag3** (c) on cellulose paper in different mole fractions of $O_{2(g)}$ in nitrogen (solid line). λ_{ex} = 325 nm. Stern–Volmer plot for the oxygen quenching of **Cu1** (d), **Cu2** (e) and **Ag3** (f) The solid lines are the best fit lines using the equation described in the experimental section.

were dried in air. A 325 nm laser line (He-Cd laser) was used as an excitation source. The phosphorescence was separated from the scattering light of the excitation pulse by an edge filter with a cut-off wavelength of 420 nm (3RD420LP, Omega Optical). N_2 (99.99%) and O_2 (99.99%) were mixed at different concentrations *via* mass flow controllers and passed into a Linkam FTIR600 stage (Linkam Scientific Instruments, United Kingdom). The O_2 concentrations were accurate to 0.1%. The output flow rate of the gas mixture was maintained at 500 mL min^{-1}.

2.5. Device fabrication

Filter paper treated with solution of **Ag3** was cut into circles of 0.5 cm diameter and placed on cell dishes. Subsequently, 40 mg sodium alginate was dissolved in 1 mL of water and then the solution was mixed with glucose oxidase in phosphate buffer solution (1 mL). The resulting solution (10 µL) was then dropped into the cell dish, and 0.2 M calcium chloride solution (10 µL) was added to the dish to form the hydrogel. 10 µL of glucose standard solution, blood plasma sample or urine was spotted onto the hydrogel, and the phosphorescence emission under irradiation at 405 nm was measured with a fiber-optic system.

2.6. Preparation of glucose solution, serum, blood and urine samples

Various concentrations of glucose solution ranging from 0.01 to 50 mM were dissolved in phosphate buffer (pH 7.0).

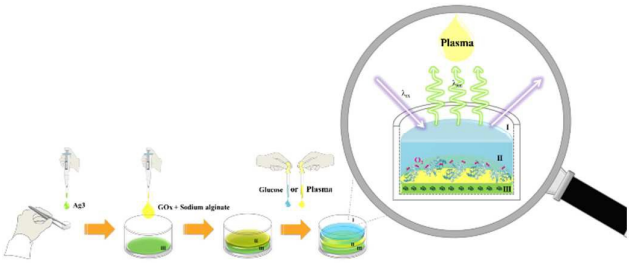

Figure 2. Schematic illustration and detection of paper-based glucose sensing: (I) dish, (II) hydrogel mixed with GOx, and (III) **Ag3** deposited on paper.

Phosphate buffer was prepared from monosodium phosphate monohydrate and disodium hydrogen phosphate (Merck). Human serum (SRM 965b) was purchased from NIST, and the glucose concentration (16 mM) in the serum was certified by isotope dilution gas chromatography mass-spectrometry.[27] The serum solutions were filtered by using the Nanosep centrifugal device with a cut-off of 3 kDa at 14,000 rpm and 4°C for 10 min to remove protein.[28] The collection and analysis of blood and urine samples was approved by the institutional review board of Taipei Veterans General Hospital (Taiwan; IRB registration number 2017-12-002CC). Blood sampling was performed with a disposable lancet, and samples were collected into anticoagulants (EDTA 1.8 g/L and NaF 3g/L). The blood plasma were collected from the upper layer containing plasma water and protein, which were then analyzed in triplicate. A mid-stream specimen of urine was collected without any further treatments. Next, glucose concentrations in buffer solution ranging from 1 to 20 mM were added to the urine sample.

2.7. Sensing detection of glucose, and analysis of glucose sensing efficiency

The luminescence detection of glucose was carried out with a bifurcated optical fiber system (QBIF600-UV-VIS, Ocean Optics) and optical data were collected using a CCD image sensor (QE65000, Ocean Optics). 10 µL of different concentrations of glucose in phosphate buffer, blood plasma or urine were respectively added into the dishes. A 405 nm LED (LLS-405, Ocean Optics) was used as the excitation source, coupled with an edge filter having a cut-off wavelength of 455 nm throughout the measurement. The fiber-optic data were collected every 200 ms for 30 s. Finally, the change in luminescence intensity and the corresponding kinetic behaviour were recorded.

The kinetic behaviour and efficiency of the **Ag3** paper-based glucose sensor, i.e., the phosphorescence change rate, were evaluated by equation (1), where I_t is the phosphorescence intensity at time t, I_0 and I_1 are the phosphorescence intensities at the beginning and on reaching saturation, respectively, and the point of inflection in the curve (t_{max}) and dt signifies the time for most significant phosphorescence changes in intensity.

View Article Online
DOI: 10.1039/C8DT00500A

Table 1. Oxygen-quenching fitting parameters of **Cu1**, **Cu2** and **Ag3** on paper and comparison of the oxygen-sensing performances of copper and silver-based compounds.

Compound	K_{SV1} (atm^{-1})	f_1	K_{SV2} (atm^{-1})	f_2	LOD, %	Ref.
Cu1	29.7	0.80	0.23	0.20	0.32%	Our work
Cu2	22.7	0.77	0.33	0.23	0.39%	Our work
Ag3	47.6	0.94	2.63	0.06	0.08%	Our work
Ag-(Pd-TPP)NF[a]	3.98				0.75%	30
Ag-Ru dye in EC[b]	0.01				N.A.[f]	31
$Ag_{12}bpy$[c]	64.7				N.A.	32
[Cu(xantphos)(dmp)]tfpb[d]	5.82				N.A.	29
[Cu(CN-xylyl)(dbp)]tfpb[e]	3.12				N.A.	26

[a]Ag-(Pd-TPP)NF, Pd-TPP-based nanofiber in presence of silver nanoparticles. [b]Ag nanoparticles containing-Ru(bipy)$_3^{2+}$ in ethylcellulose. [c]$Ag_{12}bpy$, $[(Ag_{12}(S^tBu)_8(CF_3COO)_4(bpy)_4)]_n$, bpy = 4,4'-Bipyridine. [d]crystalline [Cu(xantphos)(dmp)]tfpb, xantphos = 4,5-bis(diphenylphosphino)-9,9-dimethylxanthene, dmp = 2,9-dimethyl-1,10-phenanthroline, tfpb = tetrakis(bis-3,5-trifluoromethylphenylborate). [e]crystalline [Cu(CN-xylyl)(dbp)]tfpb, CN-xylyl = 2,6-dimethylphenyl-isocyanide, dbp = 2,9-di-tert-butyl-1,10-phenanthroline. [f] N.A. means Not Available.

$$I_t = I_1 + \frac{I_0 - I_1}{1 + e^{(t - t_{\max})dt}}$$

$$Rate = \frac{I_1}{t_{\max}} \quad (1)$$

Results and Discussion

3.1. Synthesis and structural description of Cu1, Cu2 and Ag3

Cu2 complex has been reported earlier.[26] For the sake of comparison, the structurally similar compound **Cu1** with bulkier diimine ligand (2,9-dimethyl-4,7-diphenyl-1,10-phenanthroline, Chart 1) was prepared following a similar synthetic protocol. The dinuclear triphosphine-based compound [Ag(P^3)–CN–Ag(P^3)](tfpb) (**Ag3**; $tfpb^-$ = tetrakis(bis-3,5-trifluoromethylphenylborate), Chart 1, was synthesized from its BF_4^- precursor[21] via straightforward counterion exchange using commercially available Na(tfpb) salt. The choice of the bulky anion $tfpb^-$ is dictated by the need to ensure uniformity, low density and appreciable porosity of the non-crystalline solids, which are formed on the paper support.

3.2. Molecular gas oxygen quenching ability of Cu1, Cu2 and Ag3

The relevant crystalline Cu(I) complexes have been shown to possess good gas oxygen sensing ability in neat microcrystalline forms.[21,26,29] This property was attributed to the presence of sufficient void space within the solid to allow oxygen molecules to penetrate into the bulk material and result in quenching of the excited triplet excited state of the complex by the ground state triplet oxygen via collisional interactions in the confined space.[21,26,29]

For choosing the most suitable materials among readily available **Cu1**, **Cu2** and **Ag3** for the further glucose sensing test, we first determined the Stern-Volmer quenching constants (K_{SV}) between complexes and oxygen on paper, i.e., oxygen quenching ability. As shown in Figure 1(a)–(c), at 1 atm of O_2 at room temperature, the emission intensities of **Cu1**, **Cu2** and **Ag3** were quenched by 80.88%, 79.40%, and 96.50%, respectively. The results revealed that the oxygen sensing property of **Ag3** was better than those of **Cu1** and **Cu2**. The ratios between peak intensity of the absence of oxygen (I_0) and the exposure of different concentrations of O_2 (I) against the mole fraction of O_2 in nitrogen were not linear (Figure 1(d)-(f)). Accordingly, the data were fitted by a two-site model, which is described by equation (2):

$$\frac{I_0}{I} = \left(\frac{f_1}{1 + K_{SV1}[O_2]} + \frac{f_2}{1 + K_{SV2}[O_2]} \right)^{-1}, \; f_1 + f_2 = 1 \quad (2)$$

where f_1 and f_2 denote the fractions of the total emission intensity generated by each site, and K_{SV1} and K_{SV2} are the Stern-Volmer quenching constants for the two sites. Pertinent fitting data are summarized in Table 1. Although two different environments were identified in **Cu1**, **Cu2** and **Ag3**, one site in **Ag3** constituted a significantly smaller fraction (f_2 = 0.06, i.e., 6%), which was poorly quenched by O_2 (2.63 atm^{-1}). The K_{SV1} value in **Ag3** (47.6 atm^{-1}) was higher than that of Pd-porphyrin complexes-doped and the nano-silver containing Ru(bipy)$_3^{2+}$ in ethylcellulose with silver nanoparticles, but lower than the value recently reported for a silver-chalcogenolate cluster-based metal–organic framework.[30-32]

The sensitivity of **Cu2**, which has been previously studied in crystalline form to reach a high K_{SV} value of 96 atm^{-1} and a linear Stern-Volmer relationship,[26] on paper demonstrated a substantial decrease (max K_{SV1} = 22.7 atm^{-1}), essentially due to the non-crystalline nature of the film, which was expected to give a lower effective quenching area. The minimum detectable concentrations (LODs) of oxygen for **Cu1**, **Cu2** and **Ag3** were calculated to be 0.32%, 0.39%, and 0.08%, respectively, from three times the signal to noise ratio. Taking advantage of a large K_{SV} value and its excellent stability, compound **Ag3** was employed as a paradigm for the following glucose-sensing experiments.

3.3. Design of paper-based glucose sensor

In this design, in order to fulfil the criteria of higher sensitivity and better stability than those of the electrochemical-type glucose biosensor, compound **Ag3** was chosen as the main sensing molecular material to recognize glucose. Furthermore, the large quenching constant of **Ag3** offers several advantages such as simplifying the fabrication of a glucose assay device (*vide infra*), expansion of the glucose response range and better selectivity toward glucose. As illustrated in Figure 2, a methanol solution of **Ag3** was added into the paper, which was placed on the cell dishes and then capped with enzyme hydrogel. Also, for the control test, GOx was deposited on air onto **Ag3** directly without mixing with hydrogel (see Figure S1 in the supporting information). When 20 mM of glucose was added to this device without hydrogel, the

View Article Online
DOI: 10.1039/C8DT00500A

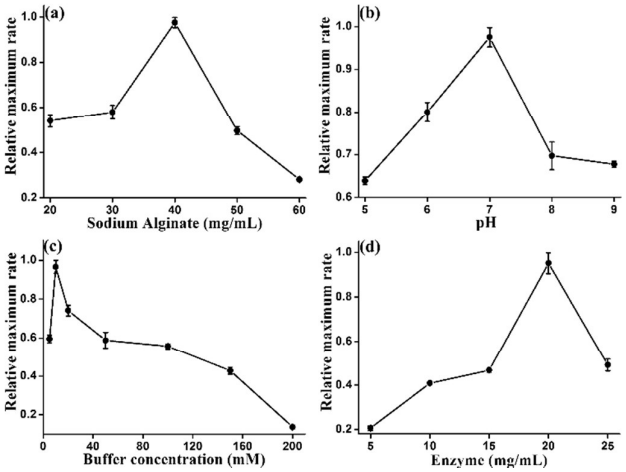

Figure 3. Effects of concentration of the sodium alginate (a), pH value and the concentration of the buffer (b and c), and concentration of the enzyme on the relative maximum emission change rate of the paper-based biosensor upon exposure to 20 mM glucose. Data were obtained from the average values of three replicated measurements (N = 3).

change in emission intensity gradually decreased, suggesting that the emission was quenched by glucose. On the contrary, when 20 mM of glucose was added to the hydrogel-capped **Ag3** on paper, the change in emission intensity gradually elevated. Therefore, when human blood glucose or urine was added to the dishes, oxygen molecules in the interior of the biosensor were consumed by GOx. As a result, upon photoexcitation of the sample with diode laser or blue OLED with suitable wavelength, the enhanced emission intensity of the **Ag3** complex was recorded and analyzed.

3.4. Optimization of the amount of sodium alginate, the effect of the concentration and pH of buffer, and the concentration of GOx

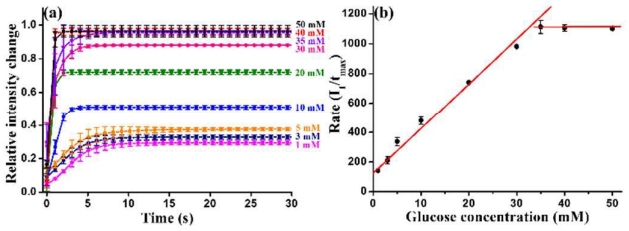

Figure 4. (a) Relative emission intensity change curves of a paper-based biosensor upon addition of different concentrations of glucose (N = 3). (b) Maximum emission change rate as a function of glucose concentration calibration curve obtained for biosensor (N = 3).

The amount of sodium alginate and gelling agent, e.g., calcium chloride, in a biosensor device should affect the degree of cross-linking and the pore size of the hydrogel.[33] Therefore, various concentrations of sodium alginate were tested to achieve the optimized emission change rate upon the addition of 20 mM glucose with 15 mg mL-1 GOx in 100 mM PBS buffer solution (pH = 7) and a fixed gelling agent concentration of 0.2 M (10 μL). The maximum emission change rate was calculated according to eqn (1). It was found that the amount of sodium alginate of 40 mg in 1 mL buffer distinctly facilitated the emission change rate in the reaction with glucose, as shown in Figure 3(a).

The effects of the concentration and pH value of the buffer on the relative change rates of the immobilized GOx are compared in Figure 3(b) and 3(c). The influences of pH value of the buffer solution in the pH range of 5.0–9.0 upon addition of 20 mM glucose with 15 mg mL-1 GOx in 100 mM PBS solution was studied. As can been seen from Figure 3(b), the maximum change rate of phosphorescence increased with the elevation of pH value and

Table 2. Comparison of the performances of the various types of optical glucose sensors.

Compounds	Linear response range (mM)	LOD (mM)	Response Time (s)	Ref.
Ag3 on paper	1.0-35.0	0.09	10.0	Our work
Ag@Au–Ir–Zn_e MOFs on paper[a]	0.05-30.0	0.038	0.5	13
Ir-Zn_e in tube	0.10-6.0	0.05	< 120	35
Ir-Zn_e on paper	0.05-8.0	0.05	0.12	28
Ir-Zn MOFs[b]	0.05-5.0	0.01	< 240	36
Ir-Cd-E-A[c]	0.05-5.0	0.01	< 240	34
GOx-GPS-SANDs in solution[d]	0.088-0.4	0.1	N.A.	37
Cu NCs in solution[e]	0.01-1	0.01	N.A.	38
BZP in solution[f]	1.1-7.0	1.10	N.A.	39
$(PAH/CdTe)_{12}(PAH/PSS)_3(PAH/GOD)_3$ film[g]	0.5–16.0	0.50	300	16
CdTe/CdS–GOx in solution[h]	0.1-7.0	0.10	N.A.	40
MoS_2 QDs in solution[i]	0.01-1.5	0.005	600	41
PBS-GQDs in solution[j]	4.0-40.0	3.00	N.A.	42
μPADs on paper[k]	0.1-1.0	0.05	900	43
GOx-HRP μPADs on paper[l]	5.0-17.0	0.30	150	44

[a]Ag@Au–Ir–Zn_e MOFs: Ag@Au nanoprism-metal–organic frameworks (MOFs). [b]Ir-Zn MOFs: $Ir(ppy)_2(H_2dcbpy)PF_6$. [c]Ir-Cd-E-A: Ir–Cd-eggmembrane-a hydrogel. [d]GOx-GPS-SANDs: GOx-3-Glycidoxypropyl trimethoxysilane-containing self-assembled SiOx nanodots. [e]Cu NCs: Copper nanoclusters. [f]BZP: 4,4'-bis(diethylamino)benzophenone hydrosol. [g]$(PAH/CdTe)_{12}(PAH/PSS)_3(PAH/GOD)_3$ film: (poly(allylamine hydrochloride)/CdTe)$_x$(PAH/sodium polystyrenesulfonate)$_y$(PAH/Glucose oxidase)$_z$ multilayer. [h]CdTe/CdS–GOx: CdTe/CdS quantum dots (QDs)–glucose oxidase (GOx) complex. [i]MoS_2 QDs: molybdenum disulfide quantum dots. [j]PBS-GQDs: phenyl boronic salt-graphene quantum dots. [k]μPADs: GOx, horseradish peroxidase, and 3, 3', 5, 5'-tetramethylbenzydine on paper. [l]GOx-HRP μPADs: GOx, horseradish peroxidase, 4-aminoantipyrine, N-Ethyl-N-(2-hydroxy-3-sulfopropyl)-3,5-dimethylaniline sodium salt monohydrate and on paper.

View Article Online
DOI: 10.1039/C8DT00500A

Table 3. The potential interfering substances in human.

Interferents	sample	The normal ranges	Ref.
D-fructose	blood	31 μM	46
Maltose monohydrate	plasma	1.2 mM	47
L-cysteine	plasma	240–360 μM	48
Glutathione	plasma	0.065 μM	49
L-phenylalanine	plasma	41.8–57.5 μM	50
Galactose	human body	1.8 μM	51
Lactose	serum	18 μM	52
Ascorbic acid	blood	34 μM	53
Citric acid	serum	54 μM	54
Uric acid	serum	0.5 mM	52
Glycine	plasma	0.49 μM	55
L-tryptophan	urine	7.8 μM	56
Potassium ion	serum	3.5–5.0 mM	57
Sodium ion	serum	135–150 mM	58
Magnesium ion	serum	0.7–0.96 mM	58
Calcium ion	serum	2.4–2.6 mM	57
L-methionine	urine	1 μM	56
L-aspartic acid	urine	10.9 μM	59
L-valine	urine	3.4 μM	56
Lauric acid	urine	0.03 μM	56

reached its maximum at 7.0. This value is slightly more acidic than free GOx in PBS solution,[34] indicating that the enzyme activity shifts to a more acidic value upon entrapment. The different buffer concentrations were studied in the range of 5.0–200 mM upon addition of 20 mM glucose with 15 mg mL-1 GOx and 40 mg mL-1 sodium alginate. It is clear from Figure 3(c) that the concentration of 10 mM exhibited the best maximum change rate.

The most suitable concentration of the immobilized enzyme GOx, ranging from 5.0 to 25 mg mL^{-1} upon addition of 20 mM glucose at an optimum pH of 7.0 in 10 mM PBS solution on the oxidation of glucose, was subsequently examined. The data in Figure 3(d) revealed that the enzyme concentration of 20 mg mL^{-1} resulted in the maximum emission change rate. Accordingly, 20 mg mL-1 GOx in 10 mM buffer solution of pH 7.0 was used in further calibration curve construction and real sample analyses.

3.5. Paper-based biosensor for glucose sensing

On the basis of the above optimized conditions, a calibration curve of glucose analysis was constructed. As shown in Figure 4(a), the intensity of the characteristic peak at 530 nm and response curve increased when the concentration of glucose increased, and the response time (i.e., oxygen exhausting) was less than 10 s, which represents a fast response as compared with other optical glucose sensors (Table 2).[13,28,34–44] Figure 4(b) shows each maximum emission change rate against different glucose concentrations. They are linear in the 1.0 to 35 mM concentration range (y = 30.19 [glucose] + 124.9, with an R^2 value of 0.9972; for N = 3). The detection limit was 0.09 mM from three times the signal-to-noise ratio. It has been noted above that this glucose concentration range is suitable for diagnosis of both normal persons (4.4–6.6 mM in blood; 0.1–0.8 mM in urine) and diabetes patients. Comparing with majority of other optical glucose sensing systems reported

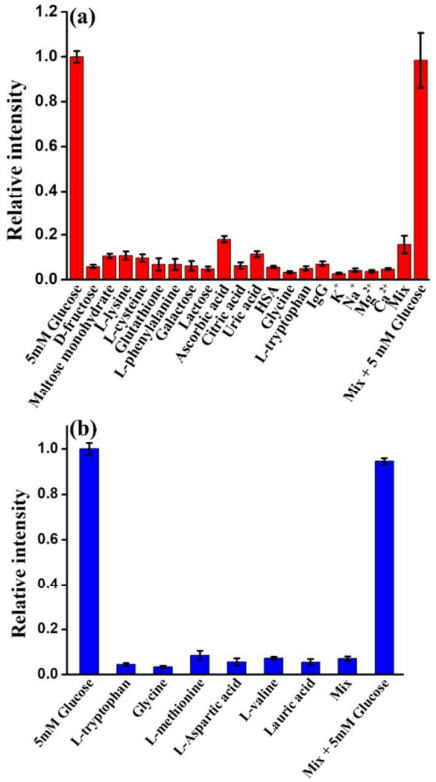

Figure 5. (a) Selectivity of paper-based biosensor toward various potential interfering substances in blood. Interference test of the glucose biosensor at pH 7.0 PBS buffer. The mixture (Mix) contained all of the interfering substances in blood. (b) The influences of common substances present in urine. The mixture (Mix) contained all of the interfering substances in urine. All of the interfering substances concentrations were 10 mM.

previously (see Table 2), the proposed method provides a wider sensing range, faster response, and good sensitivity.

Additionally, the Michaelis-Menten constant (K_m) of GOx in hydrogel was calculated by using a Lineweaver–Burke plot with glucose concentrations in the range of 3–35 mM. The K_m value was calculated to be 17.43 mM (Figure S2), which was much lower than the reported value of 33 mM of free GOx.[45] This apparently indicates that the binding affinity of the glucose was improved when the GOx was confined in hydrogel, as compared with that of free GOx in solution.

3.6. Selectivity of glucose detection

For the application of glucose detection in blood (plasma and serum) and urine, competitive molecules and/or ions in blood or urine, including D-fructose, maltose monohydrate and many others, which are listed in Table 3, are considered on the relative emission intensities of the sensing system. Their normal ranges in humans for each corresponding substances are also listed in Table 3. In this selectivity test of glucose, the concentrations of the potential interfering substances in blood (and urine) were prepared at ~10-fold (~100-fold) excess concentrations, higher than the typical normal levels in human blood and urine. The concentration of human serum albumin was 0.075 mM (saturated concentration). As shown in Figures 5(a) and 5(b), all the substances, even in mixtures

View Article Online
DOI: 10.1039/C8DT00500A

Table 4. Detection of glucose in human serum, blood plasma and urine.

Biofluids	Concentration (mM)		Glucose added (mM)	Glucose found[a] (mM)	Recovery (%)	R.S.D.[b](%)
	Claimed value	Proposed method[a]				
Human serum	16.35 ± 0.20[c]	16.40 ± 0.203				1.24
Human blood plasma	6.53 ± 0.21[d]	6.24 ± 0.04				0.64
Human blood plasma			3	3.056 ± 0.127	101.9	4.16
Human blood plasma			5	4.968 ± 0.081	99.36	1.63
Human blood plasma			10	10.04 ± 0.144	100.4	1.43
Human blood plasma			20	20.03 ± 0.393	100.2	1.96
urine			3	3.088 ± 0.114	102.9	3.69
urine			5	4.995 ± 0.182	99.90	3.65
urine			10	10.01 ± 0.248	101.0	2.48
urine			20	19.99 ± 0.252	99.90	1.26

[a] N = 3.
[b] R.S.D.: relative standard deviation.
[c] The glucose concentrations in human serum were certified by the definitive method, isotope dilution gas chromatography mass-spectrometry.[27]
[d] The glucose concentrations in human blood plasma were measured by the commercial glucometer from Roche.

of all agents interfere insignificantly with glucose determination in blood and urine. Therefore, the potential interfering substances in blood and urine could not effectively compete with glucose.

3.7. Glucose determination in human blood plasma and urine

For the performance of the proposed sensing system in practice, paper-based **Ag3** was tested in serum first. Serum is the liquid part of blood plasma without the clotting factors, e.g. fibrinogen. The certified glucose concentrations of NIST SRM965b and their uncertainty were 16.35 ± 0.20 mM (Table 4); those obtained with the proposed method were 16.40 ± 0.203 mM with R.S.D values lower than 1.24%, which indicates that the results were accurate and that the proposed method can assay intrinsic glucose molecules in serum. Next, the applicability of the proposed system for human biofluids was proven by analysing glucose in human blood plasma and urine. To prevent blood clotting, human blood was collected into anticoagulants; then blood plasma were collected before assay. The measured glucose levels was found to be 6.24 ± 0.04 mM, which is in accordance with the values from the glucometer (Roche, Accu-Chek Active), indicating that the present method has negligible interference from the protein. Urine samples were used directly without any pre-treatment. Glucose in human blood plasma and urine was determined by the standard addition method. As shown in Table 4, the measured values of the four samples in blood plasma and urine were respectively 3.056 ± 0.127, 4.968 ± 0.081, 10.04 ± 0.144, and 20.03 ± 0.393 mM; and 3.088 ± 0.114, 4.995 ± 0.182, 10.01 ± 0.248, and 19.99 ± 0.252 mM. Analysis results of R.S.D values of these four added concentrations in blood plasma and urine were respectively 4.16, 1.63, 1.43 and 1.96%; and 3.69, 3.65, 2.48 and 1.26% R.S.D., indicating that the results were feasible, accurate, and credible. The four samples in blood and urine respectively ranged from 99.36% to 101.9% and 99.9% to 102.9%, showing acceptable recovery of glucose.

3.8. Stability

Last but not least, the storage stability of this biosensor was examined during storage at 4 ^{o}C and measured for a period of 45 days. Results are shown in Figure S3. The samples were tested upon addition of 20 mM glucose, and the biosensor retained 97.78% of its initial response rate during the first 15 days. After 45 days, the paper-based samples still retained 99.75% of the initial response rate, showing excellent storage stability for the practical application.

Conclusions

Compounds **Cu1**, **Cu2**, and **Ag3** were synthesized and their oxygen-quenching abilities examined with various comparative analyses. As a result, a facile overall preparation of a paper-based glucose assay is described in this paper. This achievement was attained through the incorporation of the **Ag3** complex, which has high oxygen sensing ability and stability on paper, ensuring a more effective collision with oxygen and resulting in a wide sensing range for recognizing glucose. Moreover, this paper-based device is cost effective and provides a fast response time (10 s) for sensing glucose in a quantitative manner. The performance of the present device is superior to those of other optical glucose sensors. Furthermore, the paper-based device provides a stronger binding affinity to glucose, resulting in high specificity. The improvements in this device allow the detection of glucose in human blood and urine in high precision and reliability.

Conflicts of interest

There are no conflicts to declare.

Acknowledgements

We thank the Ministry of Science and Technology (MOST), R.O.C., for financial support (Grant 105-2113-M-031-002) and the Academy of Finland (Grant 268993 to I.O.K.).

References

View Article Online
DOI: 10.1039/C8DT00500A

1 K. Narsaiah, S. N. Jha, R. Bhardwaj, R. Sharma and R. Kumar, *J. Food Sci. Technol.,* 2012, **49**, 383-406.
2 H.-C. Wang and A.-R. Lee, *J. Food Drug Anal.,* 2015, **23**, 191-200.
3 A. K. Yetisen, N. Jiang, A. Fallahi, Y. Montelongo, G. U. Ruiz-Esparza, A. Tamayol, Y. S. Zhang, I. Mahmood, S.-A. Yang, K. S. Kim, H. Butt, A. Khademhosseini and S.-H. Yun, *Adv. Mater.*, 2017, **29**, 1606380-1606391.
4 H. Zhu, S. Mavandadi, A. F. Coskun, O. Yaglidere and A. Ozcan, *Anal. Chem.*, 2011, **83**, 6641-6647.
5 S. Liu, W. Su and X. Ding, *Sensors*, 2016, **16**, 2086–2102.
6 E. W. Nery, M. Kundys, P. S. Jeleń and M. Jönsson-Niedziółka, *Anal. Chem.*, 2016, **88**, 11271-11282.
7 Y.-C. Shiang, C.-C. Huang and H.-T. Chang, *Chem. Commun.*, 2009, **23**, 3437–3439.
8 V. Muhr, M. Buchner, T. Hirsch, D. J. Jovanović, S. D. Dolić, M. D. Dramićanin and O. S. Wolfbeis, *Sens. Actuators B Chem.*, 2017, **241**, 349–356.
9 S. Y. Lim, J. H. Kim, J. S. Lee, J. Ahn, M.-G. Kim and C. B. Park, *J. Mater. Chem.*, 2011, **21**, 17623–17626.
10 J. Liu, L. Lu, A. Li, J. Tang, S. Wang, S. Xu and L. Wang, *Biosens. Bioelectron.*, 2015, **68**, 204–209.
11 Y. He, X. Wang, J. Sun, S. Jiao, H. Chen, F. Gao and L. Wang, *Anal. Chim. Acta*, 2014, **810**, 71–78.
12 N. A. Burmistrova, O. A. Kolontaeva and A. Duerkop, *Chemosensors*, 2015, **3**, 253–273.
13 P.-H. Huang, C. P. Hong, J. F. Zhu, Z.-T. Chen, C.-T. Chan, Y.-C. Ko, T.-L. Lin, Z.-B. Pan, N.-K. Sun, Y.-C. Wang, J.-J. Luo, T.-C. Lin, C.-C. Kang, J.-J. Shyue and M.-L. Ho, *Dalton Trans.*, 2017, **46**, 6985–6993.
14 G. M. Durán, T. E. Benavidez, A. Ríos and C. D. García, *Microchim. Acta*, 2016, **183**, 611–616.
15 J. H. Yu, L. Ge, J. D. Huang, S. M. Wang and S. G. Ge, *Lab Chip*, 2011, **11**, 1286–1291.
16 X. Li, Y. Zhou, Z. Zheng, X. Yue, Z. Dai, S. Liu and Z. Tang, *Langmuir*, 2009, **25**, 6580-6586.
17 E.-H. Yoo and S.-Y. Lee, *Sensors*, 2010, **10**, 4558–4576.
18 Q. Benito, B. Baptiste, A. Polian, L. Delbes, L. Martinelli, T. Gacoin, J.-P. Boilot and S. Perruchas, *Inorg. Chem.*, 2015, **54**, 9821-9825.
19 Q. Benito, X. F. Le Goff, G. Nocton, A. Fargues, A. Garcia, A. Berhault, S. Kahlal, J.-Y. Saillard, C. Martineau, J. Trébosc, T. Gacoin, J.-P. Boilot and S. Perruchas, *Inorg. Chem.*, 2015, **54**, 4483-4494.
20 T. Hayashi, A. Kobayashi, H. Ohara, M. Yoshida, T. Matsumoto, H.-C. Chang and M. Kato, *Inorg. Chem.*, 2015, **54**, 8905-8913.
21 G. Chakkaradhari, Y.-T. Chen, A. J. Karttunen, M. T. Dau, J. Jänis, S. P. Tunik, P.-T. Chou, M.-L. Ho and I. O. Koshevoy, *Inorg. Chem.*, 2016, **55**, 2174-2184.
22 S.W. Oliver, *Chem. Rev.*, 2013, **113**, 3686-3733.
23 V. W.-W. Yam, V. K.-M. Au and S. Y.-L. Leung, *Chem. Rev.*, 2015, **115**, 7589-7728.
24 J. M. López-de-Luzuriaga, M. Monge and M. E. Olmos, *Dalton Trans.*, 2017, **46**, 2046-2067.
25 E. Cariati, E. Lucenti, C. Botta, U. Giovanella, D. Marinotto and S. Righetto, *Coord. Chem. Rev.*, 2016, **306**, 566-614.
26 C. S. Smith and K. R. Mann, *J. Am. Chem. Soc.*, 2012, **134**, 8786-8789.
27 N. Fogh-Andersen and P. D'Orazio, *Clin. Chem.*, 1998, **44**, 655-659.
28 Y.-A. Chen, F.-J. Tsai, Y.-T. Zeng, J.-C. Wang, H.-L. Chung, S.-Y. Lin, C. P. Hong, P.-H. Huang and G.-H. Lee, *J. Chin. Chem. Soc.*, 2016, **63**, 424–431.
29 C. S. Smith, C. W. Branham, B. J. Marquardt and K. R. Mann, *J. Am. Chem. Soc.*, 2010, **132**, 14079-14085.
30 E. Önal, Z. Ay, Z. Yel, K. Ertekin, A. G. Gürek, S. Z. Topal and C. Hirel, *RSC Adv.*, 2016, **6**, 9967-9977.
31 O. Ozturk, O. Oter, S. Yildirim, E. Subasi, K. Ertekin, E. Celik and H. Temel, *J. Lumin.*, 2014, **155**, 191-197.
32 R.-W. Huang, Y.-S. Wei, X.-Y. Dong, X.-H. Wu, C.-X. Du, S.-Q. Zang and Thomas C. W. Mak, *Nat. Chem.*, 2017, **9**, 689-697.
33 S. Geethanjali and A. Subash, *Enzyme Res.*, 2013, **2013**, 1-7.
34 M.-L. Ho, J.-C. Wang, T.-Y. Wang, C.-Y. Lin, J. F. Zhu, Y.-A. Chen and T.-C. Chen, *Sens. Actuators, B*, 2014, **190**, 479-485.
35 K.-Y. Cheng, J.-C. Wang, C.-Y. Lin, W.-R. Lin, Y.-A. Chen, F.-J. Tsai, Y.-C. Chuang, G.-Y. Lin, C.-W. Ni, Y.-T. Zeng and M.-L. Ho, *Dalton Trans.*, 2014, **43**, 6536-6547.
36 K.-Y. Cheng, J.-C. Wang, C.-Y. Lin, W.-R. Lin, Y.-A. Chen, F.-J. Tsai, Y.-C. Chuang, G.-Y. Lin, C.-W. Ni, Y.-T. Zeng and M.-L. Ho, *Dalton Trans.*, 2014, **43**, 2592-2600.
37 P.-Y. Lin and S. C. Hsieh, *Sens. Actuators, B*, 2017, **240**, 674-680.
38 L. Hu, Y. Yuan, L. Zhang, J. Zhao and S. Majeed, *Anal. Chim. Acta.*, 2013, **762**, 83-86.
39 P. Mazumdar, D. Das, G. P. Sahoo, G. Salgado-Morán and A. Misra, *Phys. Chem. Chem. Phys.*, 2015, **17**, 3343-3354.
40 L. Ding, B. Zhang, C. Xu, J. Huang and Z. Xia, *Anal. Methods*, 2016, **8**, 2967-2970.
41 X. Wang, Q. Wu, K. Jiang, C. Wang and C. Zhang, *Sens. Actuators, B*, 2017, **252**, 183-190.
42 M. Shehab, S. Ebrahim and M. Soliman, *J. Lumin.*, 2017, **184**, 110-116.
43 E. F. M. Gabriel, P. T. Garcia, F. M. Lopes and W. K. T. Coltro, *Micromachines*, 2017, **8**, 104-112.
44 H. J. Chun, Y. M. Park, Y. D. Han, Y. H. Jang and H. C. Yoon, *BioChip J.*, 2014, **8**, 218-226.
45 G. Fortier, M. Vaillancour and D. Bélanger, *Electroanal.*, 1992, **4**, 275-283.
46 M. Madero, S. E. Perez-Pozo, D. Jalal, R. J. Johnson and L. G. Sánchez-Lozada, *Curr. Hypertens. Rep.*, 2011, **13**, 29-35.
47 E. Garcia-Lopez, B. Anderstam, O. Heimburger, G. Amici, A. Werynski and B. Lindholm, *Periton. Dialysis Int.*, 2005, **25**, 181-191.
48 O. Rusin, N. N. St. Luce, R. A. Agbaria, J. O. Escobedo, S. Jiang, I. M. Warner, F. B. Dawen, K. Lian and R. M. Strongin, *J. Am. Chem. Soc.*, 2004, **126**, 438-439.
49 M. Iida, T. Yasuhara, H. Mochizuki, H. Takakura, T. Yanagisawa and H. Kubo, *J. Inherit. Metab. Dis.*, 2005, **28**, 49-55.
50 M. P. Brigham, W. H. Stein and S. Moore, *J. Clin. Invest.*, 1960, **39**, 1633-1638.
51 J. H. J. Huck, N. M. Verhoeven, E. A. Struys, G. S. Salomons, C. Jakobs and S. van der Knaap, *Am. J. Hum. Genet.*, 2004, **74**, 745-751.
52 N. Psychogios, D. D. Hau, J. Peng, A. C. Guo, R. Mandal, S. Bouatra, I. Sinelnikov, R. Krishnamurthy, R. Eisner, B. Gautam, N. Young, J. Xia, C. Knox, E. Dong, P. Huang, Z. Hollander, T. L. Pedersen, S. R. Smith, F. Bamforth, R. Greiner, B. McManus, J. W. Newman, T. Goodfriend and D. S. Wishart, *Plos One*, 2011, **6**, e16957-e16979.
53 B. D. Atanasova, A. C. Li, I. Bjarnason, K. N. Tzatchev and R. J. Simpson, *Am. J. Clin. Nutr.*, 2005, **81**, 130-133.
54 B. Hoppe, M. J. Kemper, M. G. Hvizd, D. E. Sailer and C. B. Langman, *Kidney Int.*, 1998, **53**, 1348-1352.
55 H. N. Christensen, P. F. J. Cooper, R. D. Johnson and E. L. Lynch, *J. Biol. Chem.*, 1947, **168**, 191-196.
56 K. Guo and L. Li, *Anal. Chem.*, 2009, **81**, 3919-3932.
57 H. Hisamoto, N. Miyashita, K. Watanabe, E. Nakagawa, N. Yamamoto and K. Suzuki, *Sens. Actuators. B Chem.*, 1995, **29**, 378-385.

View Article Online
DOI: 10.1039/C8DT00500A

Table of Contents Graphic